PAN ARCHIVES OF ACOUSTICS
Vol. **37**, No. 1, pp. 47–55 (2012)

DOI: 10.2478/v10168-012-0007-6

Optimization of the Multi-element Synthetic Transmit Aperture Method for Medical Ultrasound Imaging Applications

Yuriy TASINKEVYCH, Ihor TROTS, Andrzej NOWICKI, Marcin LEWANDOWSKI

Institute of Fundamental Technological Research, Polish Academy of Sciences
Pawińskiego 5B, 02-106 Warszawa, Poland; e-mail: yurijtas@ippt.pan.pl

(*received August 31, 2011; accepted January 23, 2012*)

The paper presents the optimization problem for the multi-element synthetic transmit aperture method (MSTA) in ultrasound imaging applications. The optimal choice of the transmit aperture size is made as a trade-off between the lateral resolution, penetration depth and the frame rate. Results of the analysis obtained by a developed optimization algorithm are presented. The maximum penetration depth and lateral resolution at given depths are chosen as optimization criteria. The results of numerical experiments carried out in MATLAB® using synthetic aperture data of point reflectors obtained by the FIELD II simulation program are presented. The visualization of experimental synthetic aperture data of a tissue mimicking phantom and *in vitro* measurements of the beef liver performed using the SonixTOUCH Research system are also shown.

Keywords: ultrasound imaging, synthetic aperture, beamforming.

1. Introduction

Synthetic aperture (SA) methods, which are widely used in radars (Perry, Martinson, 1978; Moreira, 1992) and sonars (Stergiopoulos, Sullivan, 1989; Yen, Carey, 1989), have spread on the medical ultrasound imaging application recently (Lockwood, 1998; Synnevag *et al.*, 2005; Nikolov *et al.*, 2008; Trots *et al.*, 2008), since they offer a number of advantages over conventional beamforming methods (Karaman, 1996; Jensen *et al.*, 2006). These include a higher spatial resolution due to the full dynamic focusing on the transmit and receive, lower power consumption due to the small number of elements used for ultrasound wavefield generation at each transmission and so on. The most perspective approach for ultrasound imaging is a Multi-element Synthetic Transmit Aperture (MSTA) method (Holm, 1995) which is known to be able to increase the frame rate of the imaging system providing a reasonable compromise between the penetration depth and lateral resolution at the same time, as compared to the other synthetic aperture (SA) techniques (Gammelmark, Jensen, 2003; Trots *et al.*, 2010). Since in MSTA the transmit aperture comprises several elements, the total transmitted power increases and the signal-to-noise ratio is improved as compared to the conventional synthetic transmit aperture method using a single element in transmit mode. The main concern in the MSTA is a proper choice of the transmit aperture size and shift between subsequent emissions. The paper presents the results of an experimental study of the developed optimization algorithm which makes the optimal choice of the number of elements in the transmit mode. The maximum penetration depth and lateral resolution at given (user defined) depths were considered as the optimization criteria. The optimization was carried out in the MATLAB® environment using the FIELD II (Jensen, Svendsen, 1992; Jensen, 1996) simulated synthetic aperture data of a system of point reflectors for the case of a 5 MHz 128-element linear transducer array with 0.48 mm pitch. Experimental results are presented for a tissue mimicking phantom as well as for a beef liver pattern study *in vitro*. The data were collected using the Ultrasonix SonixTOUCH Research system. Both the simulation and experimental results show that the optimal aperture size strongly depends on the required visualization depth. The paper is organized as follows: in the next section a brief overview of the MSTA methods for ultrasound imaging applications is given, in Sec. 3 the optimization problem for MSTA is stated and the developed algorithm is pre-

sented and discussed in details and in Sec. 4 the results of numerical experiments are shown.

2. The multi-element synthetic transmit aperture method

The MSTA method is a generalization of the conventional synthetic transmit aperture (STA) method, which uses a single element in, the transmit mode (Trots *et al.*, 2009). The MSTA instead uses a finite number of elements to transmit an unfocused ultrasound wave-field to emulate a single element. This allows to increase the transmitted power resulting in an improved signal-to-noise ratio and penetration depth. The main advantage of the MSTA is that it provides the full dynamic focusing both in transmit and receive modes yielding high imaging quality. The schematic diagram explaining the MSTA method is sketched in Fig. 1. At each time a transmit aperture comprised of several elements is used to emit an unfocused wave-field. The backscattered waves are received by each element of the transducer independently. Then the transmit aperture is moved along the transducer by certain number of elements N_{sh} and the emission-reception is repeated. Resulting radio frequency (RF) echo signals are digitized and stored in memory for further (off-line or real time) processing. For an N-element array and N_t elements used in the transmit mode $N \times M$ independent recordings are required to synthesize a final high resolution image, where M is the number of emissions in one data acquisition cycle. For non-overlapping apertures (yielding high gain in the frame rate of the imaging system) $M = \text{round}(N/N_t)$ if $N_{sh} = N_t$ is assumed, which case is mainly considered here. It should be noted, that if the overlapping transmit apertures are used, even a better image quality can be achieved. But in this case, the number of transmissions M increases, which leads to a frame rate decrease.

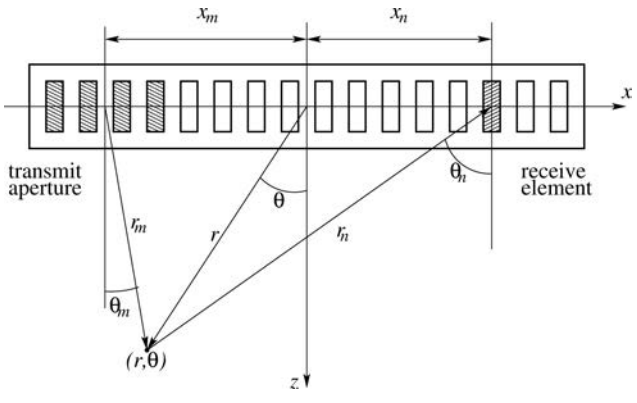

Fig. 1. The transmit and receive elements combination and the focus point in the MSTA method.

After finishing the full data acquisition cycle, the RF echo signals are summed up with properly chosen time delays according to the location of the focus point (see Fig. 1) in order to synthesize the final high resolution image. Thus, in the case of a N-element array for each point in the image, the final focused signal can be expressed as follows:

$$A_{\text{MSTA}}(r,\theta) = \sum_{m=1}^{M}\sum_{n=1}^{N} y_{m,n}\left(\frac{2r}{c} - \tau_{m,n}\right), \quad (1)$$

where $y_{m,n}(t)$ is the RF echo signal and $\tau_{m,n}$ is the round-trip delay, defined for the (m,n) transmit-receive element combination by the following expression:

$$\tau_{m,n} = \tau_m + \tau_n, \qquad 1 \le m, \quad n \le N. \quad (2)$$

The corresponding delays for m-th transmit and n-th receive elements relative to the imaging point $(r,\,\theta)$ are:

$$\tau_i = \frac{1}{c}\left(r - \sqrt{r^2 + x_i^2 - 2x_i r\sin\theta}\right), \quad i = m,n, \quad (3)$$

where x_m, x_n are the positions of the m-th transmit and n-th receive apertures, respectively, and r, θ are the polar coordinates of the imaging point with respect to the origin placed in the center of the transducer's aperture. The frame rate is increased in the MSTA with non-overlapping apertures by N_t as compared to the STA method due to decrease of the total number of emissions. This speeds up the data acquisition process considerably. Unfortunately, it appears that too excessive increasing of the transmit aperture size N_t (and its shift at the same time) leads to the lateral resolution deterioration. However, using a small number of elements in the transmit mode allows to increase the system frame rate as compared to the STA method, and provides the best compromise between penetration depth and lateral resolution. The latter strongly depends on the transducer acoustic field and is discussed in (Nowicki *et al.*, 2007). The optimal choice of the transmit aperture size is crucial in the MSTA method.

3. Optimization problem for MSTA

In this section the algorithm for optimal choice of the transmit aperture size in the MSTA method is discussed. Here we consider the case of non-overlapping transmit apertures, which means that the shift between subsequent transmissions $N_{sh} = N_t$, N_t being the number of elements used in transmit mode. The developed algorithm, however, can be extended to the more general case of the MSTA method with different values of the shift N_{sh}. Usually, $N_{sh} < N_t$ yields some improvement of the synthesized image quality at the cost of the frame rate decrease.

In the developed algorithm the maximum penetration depth and the best lateral resolution at a given depths are chosen as the optimization criteria. A test

synthetic aperture data of point reflectors was simulated in the Field II program for Matlab® for each size of the transmit aperture. The reflectors were located in the nodes of a rectangular grid. The rows and columns were equidistantly spaced. For each individual experiment the lateral resolution and penetration depth were estimated. The lateral resolution was evaluated for each lateral cross-section coinciding with the rows of the reflectors. Only the reflector located at the central column (coinciding with transducer center) was taken into account for simplicity. For convenience, the lateral cross-sections were labelled in accordance with the row numbers of the point reflectors. The lateral resolution (LR in Fig. 2a) in the presented algorithm was estimated by the full width (expressed as a number of image lines) at a given level (0.1 in the examples considered in the next section) for the reflector located at an intersection of a given row and the central column of point reflectors (see Fig. 2 for explanation).

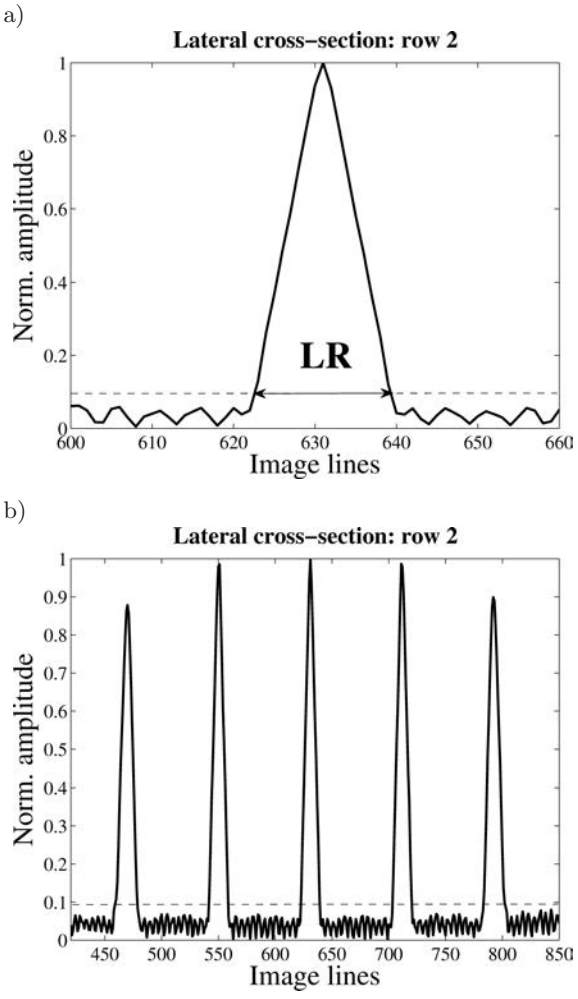

Fig. 2. Evaluation of the lateral resolution for a given row: a) LR is a full width expressed as the number of image lines at a given level (0.1 in the considered example) for the reflector located at the intersection of the row and central column of point reflectors; b) lateral cross-section of the entire given row of point reflectors.

The penetration depth was estimated in a similar manner. For the central column of point reflectors, the penetration depth (PD in Fig. 3) was assessed by the relative amplitude of the scattered signal of the deepest "visible" reflector, which means that its normalized (with respect to the maximum value in the considered axial cross-section) amplitude exceeded a certain level respective to the value of the first row (0.2 is assumed in the examples of the next section). This is illustrated in Fig. 3.

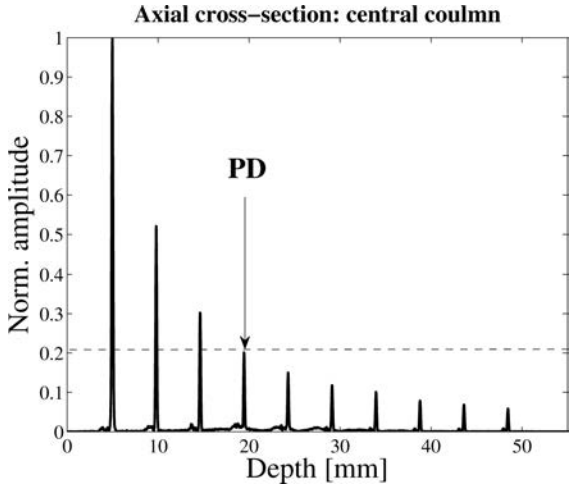

Fig. 3. Evaluation of the penetration depth: PD is the location of deepest reflector for which the normalized amplitude exceeds the given level in the axial cross-section coinciding with the central column of point reflectors.

Below this level the reflectors were assumed to be indistinguishable. In the examples explaining the optimization algorithm performance (see Figs. 2 and 3), the STA algorithm was exploited for visualization, that is a single element was used in the transmit mode. For smooth visualization of the lateral cross-sections, the interval between subsequent image lines was chosen 0.1 of the transducer pitch (10 image lines per transducer pitch) yielding the total number of 1280 image lines altogether. After estimation of the lateral resolution and penetration depth, the optimal system configuration was selected. Two different approaches were realized in the presented algorithm. The first one sought for the transmit aperture configuration yielding the maximum penetration depth for the lateral resolution being within some tolerance bounds. The second approach, on the other hand, selected the configuration giving the best lateral resolution for the penetration depth not less than some minimum acceptable limit.

In the first approach the lateral resolution was of main concern. The algorithm in the first step selected the transmit apertures yielding the lateral resolution falling within a certain defined tolerance limit. In the examples considered in the next section, the 15% acceptable decrease of the lateral resolution was

assumed. From this set of transmit aperture configurations that was selected which yielded the maximum penetration depth.

In the second approach the value of main importance was the penetration depth. The algorithm sought for the transmit apertures yielding the penetration depths not less than a certain defined minimum acceptable limit. In the example considered further this decrease was chosen to be 15% of the maximum value. From this set of transmit aperture configurations that was selected, which yielded the best lateral resolution. If more than one has been chosen (it is less likely to happen for a larger number of image lines per pitch, which directly follows from the LR definition, see Fig. 2b.) then that with the largest aperture size or, alternatively, that giving the best frame rate (minimum number of transmissions) was picked up.

4. Numerical results and discussion

In this section, the results of the simulations performed with the FIELD II program for Matlab® are presented and compared with those obtained experimentally.

4.1. FIELD II simulation

In this section the numerical results illustrating the optimization algorithm performance are presented. A 5 MHz 128-element linear transducer with 0.48 mm pitch and 0.15 mm kerf excited by one sine cycle burst pulse was considered. The FIELD II simulated synthetic aperture data of the point reflectors discussed in the previous section were used to verify the performance of the developed optimization algorithm. The reflectors were placed in the nodes of a rectangular grid comprising 10 equidistantly spaced rows and 3 columns. The central vertical line coincided with the transducer aperture centre. The reflectors were spaced 15 mm laterally and 5 mm axially The correction of RF echo signals accounting for the receive element directivity was applied in the considered MSTA method (Trots *et al.*, 2010).

In Table 1 the optimized values of the transmit aperture width N_t are shown for different visualization depths. The results correspond to the case of optimization approach selecting the configuration with maximum penetration depth from within the set of transmit apertures yielding the lateral resolution decrease less than 15% of its maximum value.

Table 1. Aperture width for different visualization depth: approach 1.

D [mm]	5	10	15	20	25	30	35	40	45	50
N_t	1	1	2	2	3	3	3	4	4	4
δLR [%]	45	52	22	16	5	12	11	–	–	–

As seen from Table 1, the maximum penetration depth was achieved with $N_t = 4$. For this configuration the decrease in the lateral resolution δLR as compared to the optimized value of N_t at different depths is shown in the last row in Table 1. The best lateral resolution was achieved with the STA algorithm using a single-element transmit aperture, but only for visualization depths not exceeding 10–15mm. On the other hand, the configuration with $N_t = 4$ enabled the visualization of the deepest parts of the phantom, but at the cost of a lateral resolution decrease at lower depths in comparison with the STA method, as seen from the last row in Table 1.

In Table 2 the optimization results are shown for the second approach selecting the configuration which yielded the best lateral resolution from the set of transmit apertures for which the penetration depth was not less than 15% of its maximum value. Comparison of the results in Table 1 and 2 reveals a similarity of the optimal transmit aperture configurations obtained by two different approaches.

Table 2. Aperture width for different visualization depth: approach 2.

D [mm]	5	10	15	20	25	30	35	40	45	50
N_t	1	2	2	3	3	3	4	4	4	4
δLR [%]	45	32	22	–	5	12	–	–	–	–

In Fig. 4 the lateral cross-sections at the depths 10, 20, 30 and 40 mm, corresponding to different optimal transmit aperture configurations, are shown. The cases of $N_t = 1{-}4$ are compared.

As can be seen from Fig. 4 for row #2 of point reflectors (10 mm depth) the optimal lateral resolution is achieved by the STA algorithm using a single-element transmit aperture, whereas at the depths of 20 mm and deeper the larger transmit apertures are the best choices. For depths exceeding 30 mm the best overall quality – the lateral resolution and penetration depth – is yielded by the transmit aperture with $N_t = 4$. This can be seen in Fig. 5 where the axial cross-sections of the central column of point reflectors are shown at different depths. Apparently, at the depths not exceeding 15–20 mm, the smaller transmit apertures give a better lateral resolution. To visualize the deeper parts of the phantom, the larger apertures should be chosen, which allows to increase the frame rate at the same time. Thus, if the main concern is the penetration depth together with the frame rate gain and some decrease in the lateral resolution is acceptable, than it is reasonable to use the MSTA algorithm with optimal number of elements $N_t = 4$ (for the considered test system of point reflectors) in the whole range of the visualization depths. In Fig. 6a, the 2D ultrasound images of the system of point reflectors are shown. The synthetic aperture data were simulated by FIELD II for the 5 MHz

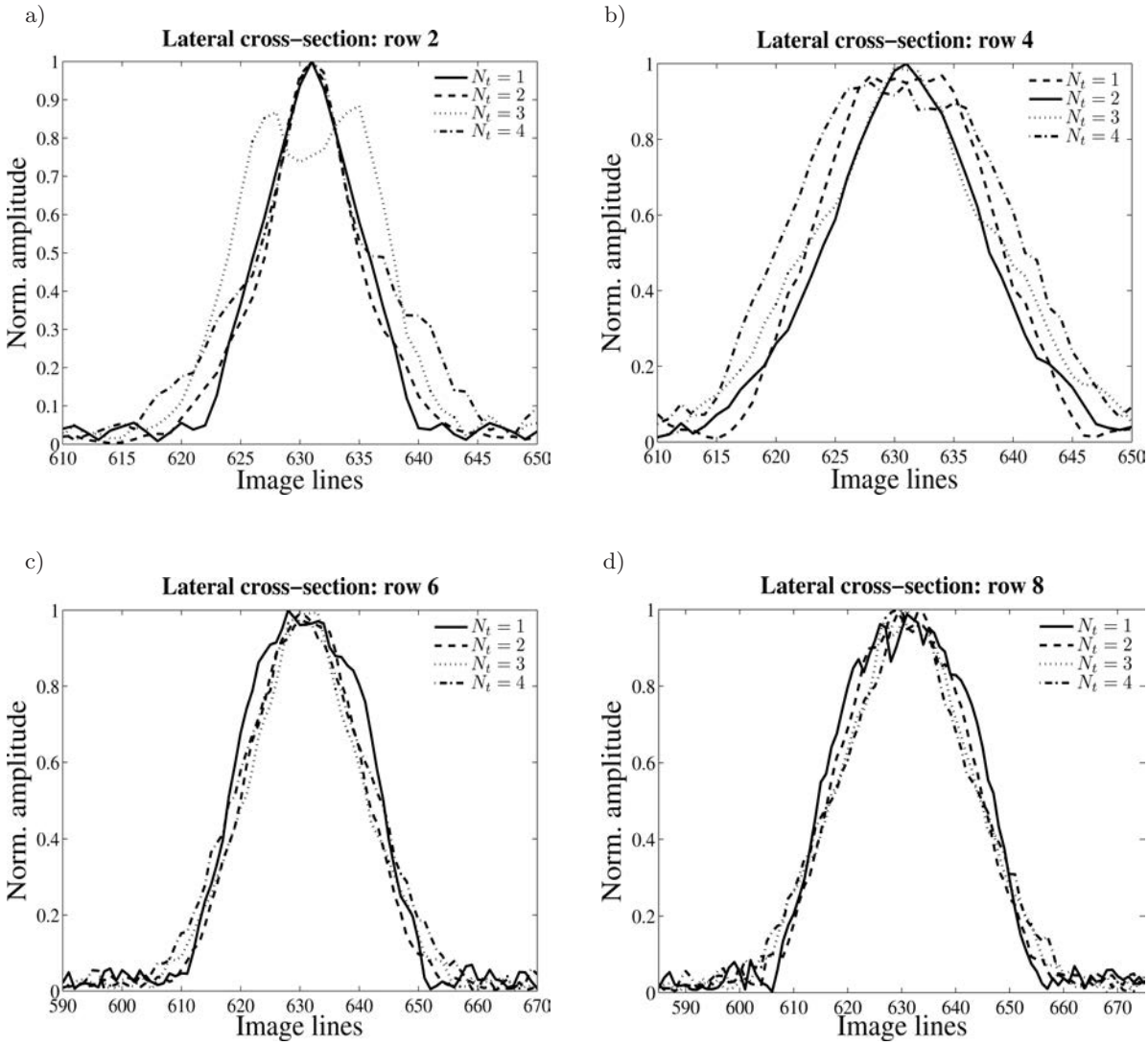

Fig. 4. Comparison of the lateral cross-sections at different depths: a) 10 mm (row #2), b) 20 mm (row #4), c) 30 mm (row #6), d) 40 mm (row #8).

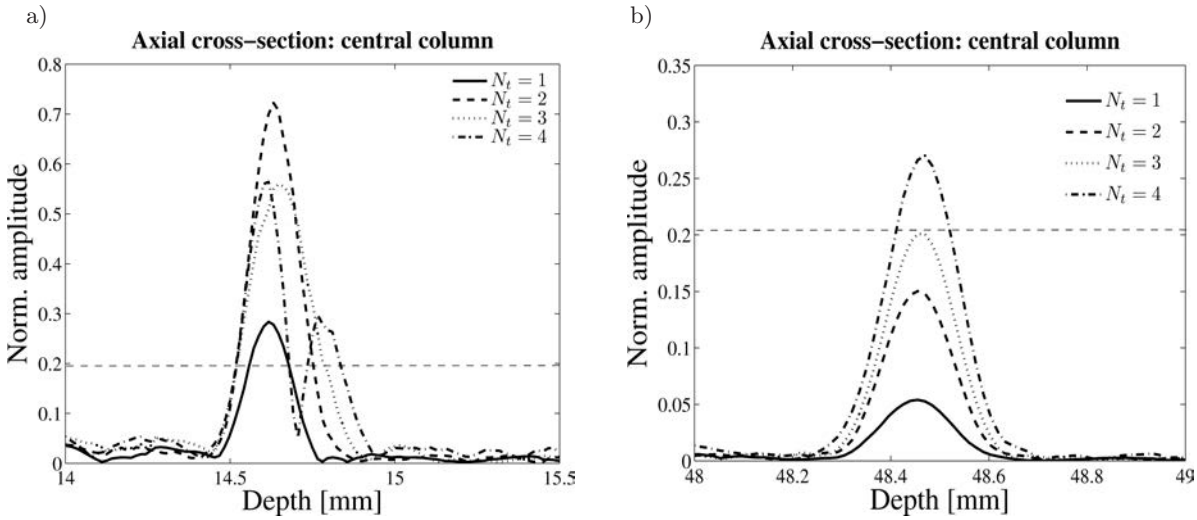

Fig. 5. Comparison of the axial cross-sections of central column of point reflectors for different depths corresponding to: a) row #3 and b) row #10.

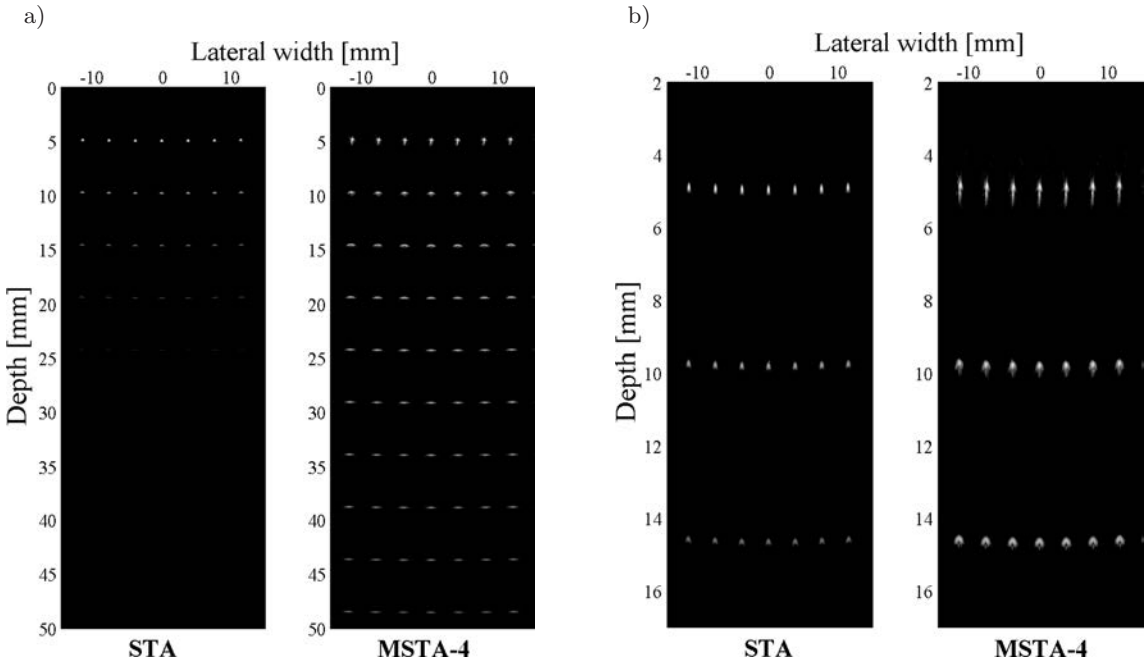

Fig. 6. 2D visualization of point reflectors using Filed II simulated synthetic aperture data a) full range of depth and b) first 3 rows; all images are displayed over 20 dB dynamic range.

128-element transducer array with a 0.48 mm pitch, excited by one sine cycle pulse burst. In Fig. 6b, the detailed view of the first three rows of point reflectors is shown. The STA algorithm is compared with MSTA using 4 elements in the transmit mode. As seen from Fig. 6, the STA algorithm yields a better lateral resolution in the vicinity of the transducer surface but a worse penetration depth as compared to the MSTA with $N_t = 4$.

4.2. Experimental results

In this section, the performance of the developed algorithm was tested using the experimentally obtained synthetic aperture data of a tissue mimicking phantom and a beef liver pattern (*in vitro* study). The measurements were done using the Sonix-TOUCH Research system (Ultrasonix Medical Corporation) equipped with a 4 MHz 128 element linear transducer L14-5/38 with a 0.3 mm element pitch, 0.28 mm element width and 70% fractional bandwidth.

In Fig. 7, the 2D ultrasound images of tissue mimicking phantom (model 525 Danish Phantom Design with attenuation of background material 0.5 dB/[MHz×cm]) are shown. As seen from Fig. 7, the optimal correlation between the penetration depth and lateral resolution was obtained by MSTA-4 with $N_t = 4$ elements in the transmit mode. The STA method is characterized by the best lateral resolution at lower depths but has a poor penetration depth. For larger apertures, $N_t = 8, 16$, the lateral resolution was worsened and the gain in penetration depth was negligible. To estimate the penetration depth and lateral resolution, the axial cross-sections of the image line #1885 (corresponding to the vertical line of reflectors in Fig. 7) and the lateral cross-sections at depths 10 and 60 mm of the above phantom for different transmit apertures are shown in Fig. 8.

As seen from Fig. 8a, at the depth of 30 mm the scattered amplitude in the case of MSTA-4 (optimal aperture) is 1.46 and 1.59 times larger than for MSTA-16 ($N_t = 16$) and STA ($N_t = 1$), whereas, in Fig. 8b one can observe that at the depth of 40 mm MSTA-4 yields 1.14 and 2.84 times larger amplitude than MSTA-16 and STA, respectively. The lateral resolution, estimated from the lateral cross-sections at the 0.3 level of its maximum value at different depths, was best in the case of the STA algorithm, as expected. Thus, at the depth of 10 mm, Fig. 8c, the STA method gives a 3% and 20%, and at the depth of 60 mm, Fig. 8d, a 3% and 8% better lateral resolution than MSTA-4 and MSTA-16, respectively.

In Fig. 9a, the 2D ultrasound images of the beef liver pattern study in vitro for different transmit aperture sizes are shown. The data were collected as above using the Ultrasonix SonixTOUCH Research system. The fresh beef liver sample was obtained from the local butcher shop within 6–8 hours after slaughter. It was refrigerated until being transferred to the lab. Ultrasonic experiments were conducted within 7–9 hours of the removal of the liver from the animal. The bovine liver sample was immersed in water at room temperature during the measurements.

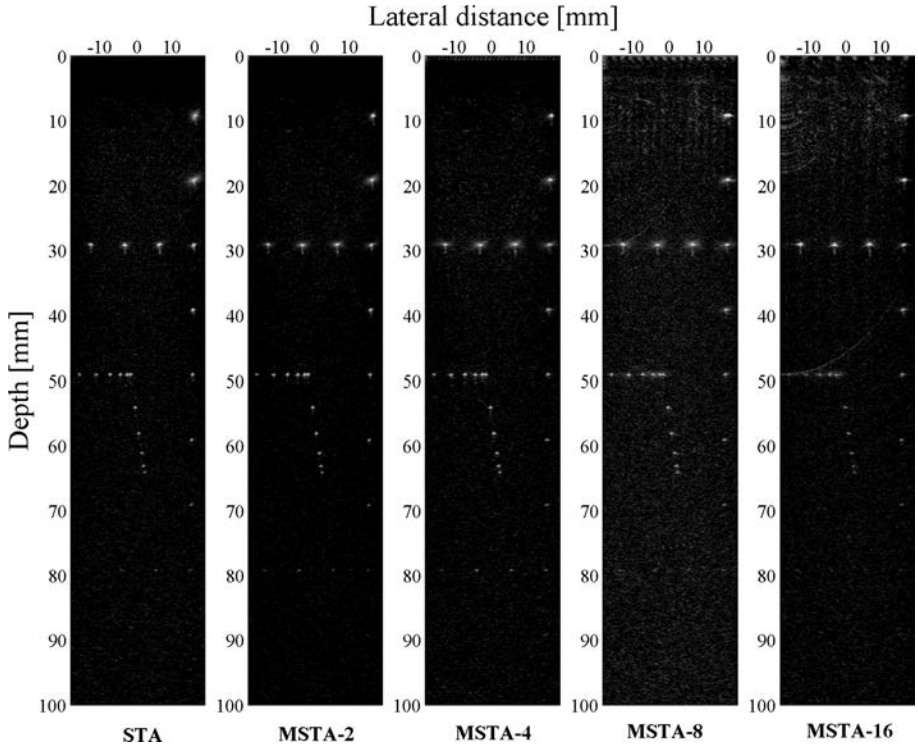

Fig. 7. 2D visualization of a tissue mimicking phantom for different transmit aperture sizes: a single-element aperture – STA and 2,4,8,16-element aperture (MSTA). All images are displayed over the 30 dB dynamic range.

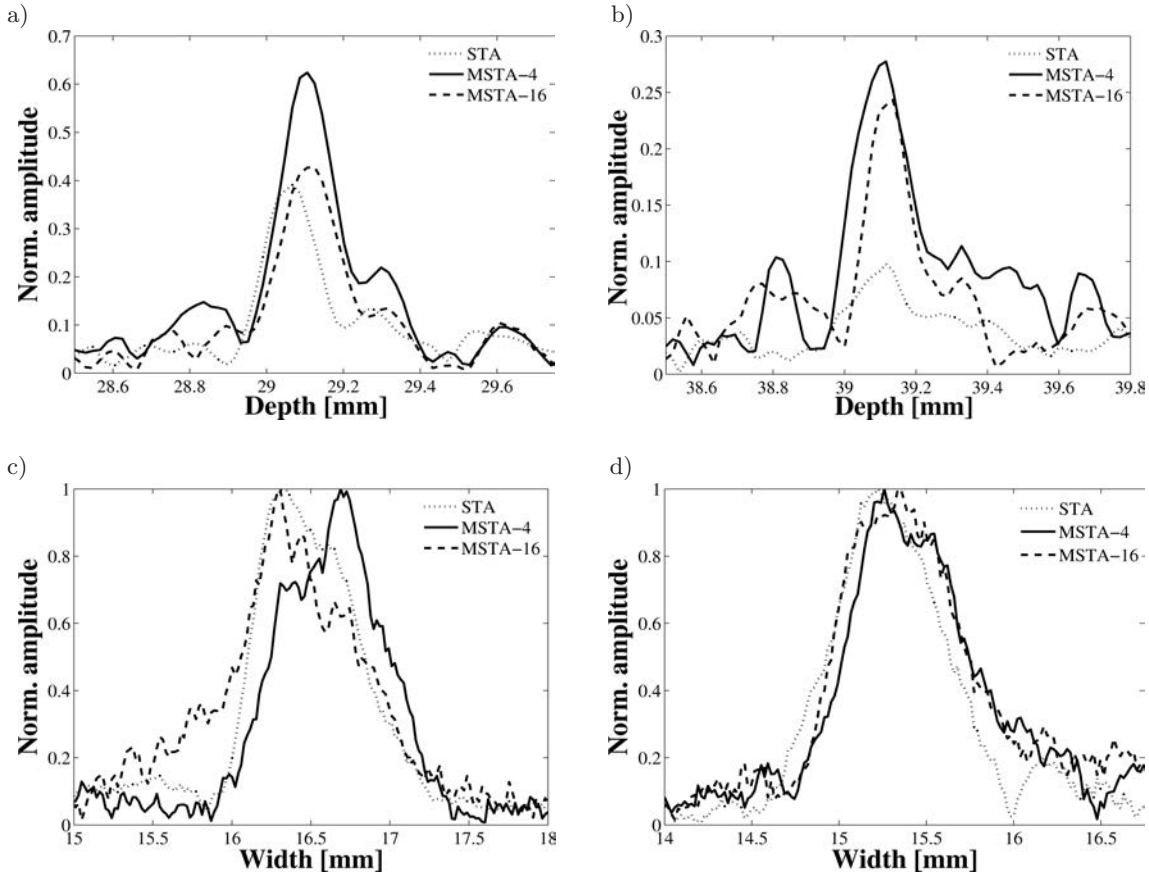

Fig. 8. a), b) Axial cross-sections of the phantom line #1885 at different depths and c), d) lateral cross-sections at depths 10 mm and 60 mm of the reflectors situated on the right hand side of the phantom. The transmit apertures with $N_t = 1, 4, 16$ are compared.

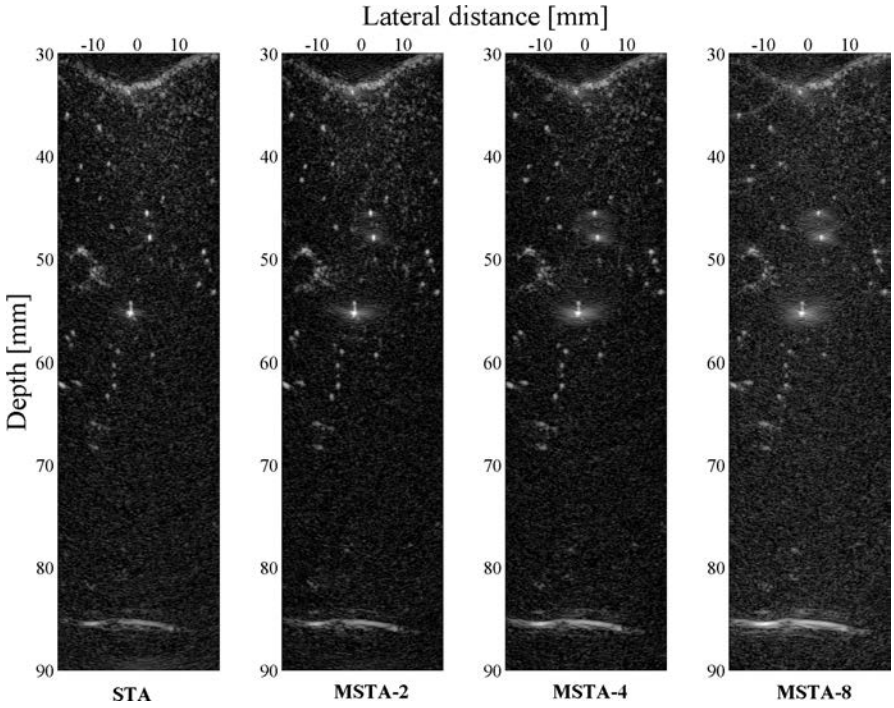

Fig. 9. 2D visualization of beef liver pattern study *in vitro* for different transmit aperture sizes: a single-element aperture – STA and 2,4,8-element aperture (MSTA). All images are displayed over the 40 dB dynamic range.

As seen in Fig. 9, the air bubbles are observed, what was almost impossible to avoid in case of *in vitro* experiments. But here they were helpful for qualitative estimation of the image quality parameters like the lateral resolution and contrast. At the same time the basic liver structure was unchanged in the presented experimental results. As expected, the STA algorithm, using a single-element transmit aperture, was characterized by the best image resolution, but the penetration depth was poor. In the case of MSTA-4 with $N_t = 4$, the optimal correlation between resolution and penetration depth was achieved at the depths up to 80–90 mm. For MSTA with a larger aperture, $N_t = 8$, the increase of the visualization depth was almost indistinguishable, whereas some degradation of the image resolution was observed.

5. Conclusions

In the work, the optimization of the multi-element synthetic transmit aperture (MSTA) method for ultrasound imaging is discussed. The transmit aperture size providing the best compromise between the lateral resolution and penetration depth of the resulting 2D ultrasound image and maintaining high frame rate at the same time is the main concern of the present study. For this purpose the corresponding optimization algorithm was developed and tested using the FIELD II simulated synthetic aperture data of point reflectors and the experimentally obtained data of the tissue mimicking phantom. For the test phantom, the best image quality as concerns the lateral resolution at low depths up to 30 mm was achieved by the small apertures with $N_t = 1, 2$. On the other hand, the deeper phantom regions (up to 90 mm) were better visualized with $N_t = 4{-}5$ elements in the transmit mode. This was also confirmed by the *in vitro* study of the beef liver pattern.

In the paper, the MSTA method with non-overlapping transmit apertures, assuming $N_{sh} = N_t$, was considered. However, the developed optimization algorithm can be generalized to the case of MSTA with $N_{sh} < N_t$, which is characterized by a somewhat better imaging quality but worse frame rate as compared to $N_{sh} = N_t$. This, however, requires some modification of the optimization criteria and is a problem of the future study. Also, the correction of RF echo signals accounting only for the single-element receive aperture directivity was applied in the considered MSTA method (Trots *et al.*, 2010). In order to account for the multi-element transmit aperture the proper modification of the MSTA method is required. To this end the results of the full-wave analysis of the radiation and scattering problem for a periodic (Tasinkevych, Danicki, 2010; Tasinkevych, Danicki, 2011) or a finite (Tasinkevych, 2010) baffle system can be applied for the purpose of modelling the directivity properties of the transmit aperture comprising several elements. The method is based on the BIS-expansion (Bloteker *et al.*, 1973), which was successfully applied to solving electrostatic problems in the theory of surface acoustic wave transducers (Danicki, Tasinkevych, 2006), in the theory

of elastic wave scattering by periodic cracks (Danicki, 2002) and in the theory of EM scattering by periodic structures (Tasinkevych, 2008; 2009; 2011). The main advantage of the above mentioned approach is that the mutual interactions of array elements are accounted for in the full-wave analysis of the corresponding mixed boundary value problem. This is another problem of future study concerning the application of the MSTA method in ultrasound imaging.

Acknowledgments

This work was supported by the Polish Ministry of Science and Higher Education (Grant NN518418436).

References

1. Blotekjaer K., Ingebrigtsen K.A., Skeie H. (1973), *Methods for analyzing waves in structures consisting of metal strips on dispersive media*, IEEE Trans. Electron. Devices, **ED20**, 12, 1133–1138.
2. Danicki E.J. (2002), *Scattering by periodic cracks and theory of comb transducers*, Wave Motion, **35**, 4, 355–370.
3. Danicki E.J., Tasinkevych Y. (2006), *Nonstandard electrostatic problem for strips*, J. Electrostat., **64**, 6, 386–391.
4. Gammelmark K.L., Jensen J.A. (2003), *Multielement synthetic transmit aperture imaging using temporal encoding*, IEEE Trans. Med. Imag., **22**, 4, 552–563.
5. Jensen J.A. (1996), *Field: A Program for Simulating Ultrasound Systems*, 10th Nordic-Baltic Conference on Biomedical Imaging Published in Medical & Biological Engineering & Computing, **34**, 1, Part 1, 351–353.
6. Jensen J.A., Svendsen B. (1992), *Calculation of pressure fields from arbitrarily shaped, apodized, and excited ultrasound transducers*, IEEE Trans. Ultrason., Ferroelectr., Freq. Contr., 39, 262–267.
7. Jensen J.A., Nikolov S.I., Gammelmark K.L., Pedersen M.H. (2006), *Synthetic aperture ultrasound imaging*, Ultrasonics, **44**, e5–e15.
8. HOLM S. (1995), *Focused multi-element synthetic aperture imaging*, Department of Informatics, University of Oslo.
9. Karaman M., Li P.C., O'Donnell M. (1995), *Synthetic aperture imaging for small scale systems*, IEEE Trans. Ultrason., Ferroelectr., Freq. Cont., **42**, 3, 429–442.
10. Lockwood G.R., Talman J.R., Brunke S.S. (1998), *Real-time 3-d ultrasound imaging using sparse synthetic aperture beamforming*, IEEE Trans. Ultrason., Ferroelectr., Freq. Cont. **45**, 4, 980–988.
11. Moreira A. (1992), *Real-time synthetic aperture radar (SAR) processing with a new subaperture approach*, IEEE Trans. Geosci. Remote Sens., **30**, 4, 714–722.
12. Nikolov S.I., Jensen J.A., Tomov B.G. (2008), *Fast parametric beamformer for synthetic aperture imaging*, IEEE Trans. Ultrason., Ferroelectr., Freq. Cont., **55**, 8, 1755–1767.
13. Nowicki A., Klimonda Z., Lewandowski M., Litniewski J., Lewin P.A., Trots I. (2007), *Direct and post-compressed sound fields for different coded excitation*, Acoustical Imaging, **28**, 399–407.
14. Perry R.M., Martinson L.W. (1978), *Radar matched filtering*, Radar Technology, Artech House, Boston, Ch. 11, 163–169.
15. Stergiopoulos S., Sullivan E.J. (1989), *Extended towed array processing by an overlap correlator*, J. Acoust. Soc. Am., **86**, 1, 158–171.
16. Synnevag J.F., Austeng A., Holm S. (2005), *Minimum variance adaptive beam-forming applied to medical ultrasound imaging*, Proc. 2005 IEEE Ultrason. Symp., 1199–1202.
17. Trots I., Nowicki A., Lewandowski M. (2008), *Laboratory setup for synthetic aperture ultrasound imaging*, Archives of Acoustics, **33**, 4, 573–580.
18. Trots I., Nowicki A., Lewandowski M. (2009), *Synthetic transmit aperture in ultrasound imaging,* Archives of Acoustics, **34**, 4, 685–695.
19. Trots I., Nowicki A., Lewandowski M., Tasinkevych Y. (2010), *Multi-element synthetic transmit aperture in medical ultrasound imaging*, Archives of Acoustics, **35**, 4, 687–699.
20. Tasinkevych Y. (2008), *Scattering of H-polarized wave by a periodic array of thick-walled parallel plate waveguides*, IEEE Trans. Antennas Propagat., **56**, 10, 3333–3337.
21. Tasinkevych Y. (2009), *EM scattering by the parallel plate waveguide array with thick walls for oblique incidence*, J. Electromagn. Waves Appl., **23**, 11-12, 1611–1621.
22. Tasinkevych Y., Danicki E. (2010), *Full-wave analysis of periodic baffle system in beamforming applications*, Archives of Acoustics, **35**, 4, 661–675.
23. Tasinkevych Y. (2010), *Wave generation by a finite baffle array in applications to beam-forming analysis*, Archives of Acoustics, **35**, 4, 677–686.
24. Tasinkevych Y., Danicki E.J. (2011), *Wave generation and scattering by periodic baffle system in application to beam-forming analysis*, Wave Motion, **48**, 2, 130–145.
25. Tasinkevych Y. (2011), *Electromagnetic Scattering by Periodic Grating of Pec Bars*, J. Electromagn. Waves Appl., **25**, 5–6, 641–650.
26. Yen N.C., Carey W. (1989), *Application of synthetic aperture processing to towed-array data*, J. Acoust. Soc. Am., **86**, 2, 754–765.